Catalysis Letters
https://doi.org/10.1007/s10562-020-03307-8

Mesoporous Sn(IV) Doping DFNS Supported $BaMnO_3$ Nanoparticles for Formylation of Amines Using Carbon Dioxide

Jie Yang[1] · Liujie Wang[1] · Aili Sun[2] · Rahele Zhiani[3]

Received: 24 April 2020 / Accepted: 1 July 2020

Abstract

In the present paper, Sn(IV) doping DFNS (SnD) supported nanoparticles of $BaMnO_3$ ($BaMnO_3$/SnD) and using as a catalyst for the *N*-formylation of amines by CO_2 hydrogenation. In this catalyst, the SnD with the ratios of Si/Sn in the range of from 6 to 50 were obtained with method of direct hydrothermal synthesis (DHS) as well as the nanoparticles of $BaMnO_3$ were on the surfaces of SnD in situ reduced. Scanning electron microscope (SEM), X-ray diffraction (XRD), Fourier transform infrared spectroscopy (FT-IR), X-ray energy dispersive spectroscopy (EDS), and transmission electron microscopy (TEM) were utilized for characterizing the nanostructures $BaMnO_3$/SnD. It is found that the nanostructures of $BaMnO_3$/SnD can be a nominate due to its effective and novel catalytic behavior in *N*-formylation of amines through hydrogenation of CO_2.

Graphic Abstract

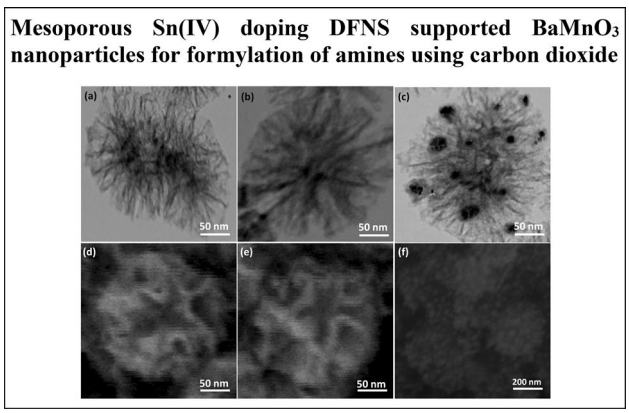

Keywords Nano catalyst · $BaMnO_3$ · *N*-formylation · Green chemistry · CO_2

1 Introduction

The transformation of carbon dioxide into useful organic chemicals is becoming an increasingly popular research topic [1–5]. It is not just one of the greenhouse gas emissions or a waste compound that coming from transportation sector, chemical industry, and power plants [6, 7], but also a non-flammable, easily available, non-toxin, and inexpensive carbon feedstock [8, 9]. Nevertheless, CO_2 is not commonly utilized in the industry, due to its low reactivity, obviously. However, CO_2 is not widely used in

✉ Aili Sun
1838770591@qq.com

✉ Rahele Zhiani
R_zhiani2006@yahoo.com

[1] College of Chemistry and Chemical Engineering, Xinxiang University, Xinxiang 453003, Henan, China

[2] Henan Engineering Laboratory of Nano-carbon Modification Membrane Technology, Xinxiang University, Xinxiang 453003, Henan, China

[3] Department of Chemistry, Faculty of Sciences, Neyshabur Branch, Islamic Azad University, Neyshabur, Iran

Published online: 22 July 2020

the industry, obviously because of its low reactivity. Substantial energy input, highly active catalysts and optimum reaction conditions are necessary for successful conversion of thermodynamically stable CO_2 molecules [10–12].

For many different applications, the industrial formamides syntheses from the *N*-formylation of amines were carried out on a large scale. Formamides are utilized as feedstock and solvents for synthesizing pharmaceutical drugs, pesticides, and herbicides. The carbonyl of formamide moiety was synthesized utilizing like acetic formic anhydride, chlorals, and formic acid, hazardous artificial reagents as carbon monoxide. Alternatively, the reductive functionalization of carbon dioxide provides an environmentally benign approach to their syntheses. The negative influences of this approach may be minimized utilizing hydrogen (H_2) instead of the more poisonous reductive parameters of silane as well as borane for *N*-formylation [13–27].

Manganese compounds are known as the impressive natural reactant used through the eubacterium and seaweed as well as herbs in the case of the water oxidation. It called the oxygen-evolving complex [28]. The water oxidation is an important reaction in unnatural light-reaction for reducing carbon dioxide (CO_2) and fabricating hydrogen [29]. Different compositions of manganese were used in diverse (e.g., areas magnetite, electro-chemistry, catalyzer, and electrochemical cells) [30–32]. Manganese is determined to be a remarkable transformation element that requires the extension of survival and living creatures. The chemical compounds that are based on manganese possess electron transfer (ET), which is a basic approach on physiological system [33]. This group of material have been highly regarded by many scholars because of the fascinating properties of $AMnO_3$ (A = Ca, Sr, Ba), [34]. An outdated and beneficial approaches in the case of Mn compounds is solid-state reaction [35]. This traditional process requires high heats (about 1400 °C) and extended devices. Due to the implementation reaction, production of a pure phase of the compound still needs more investigations. Recently, scholars used the effortless chemical methods such as sol–gel and precipitation method for the synthesizing certain mineral solids. The complex approach and the high-cost precursor are limitations of these processes [36–38]. The ultrasonic method diminished these problems. The sonochemical method has been introduced as a considerable instrument for fabricating novel nanomaterials [39]. The ultrasonic effects happen of acoustic cavitation that is the growth, implosive and construction destruction of bubbles into a solvent. The increase of the bubble happens during the dispersion of solute vapor in the volume of the bubble, while the collapse of the bubble transpires while the bubble dimension approaches its highest value. The high temperatures above 5000 K may be made over the bubble destruction based on hot spot theory [40].

In the Ref. [41], scholars stated that, because of the ordered mesoporous structure along with high surface dispersion of Sn(IV), the centers of Sn(IV) incorporated whiten the MCM-41 molecular sieve framework using the direct hydrothermal synthesis (DHS) approach that resulted in active production of catalysts (Sn-MCM-41) in the Baeyer–Villiger oxidation by an appropriate conversion as well as high chemoselectivity. Hence, for constructing impressive catalyst to catalyze the PDO oxidation, another approach of incorporating the promoters (Sn(IV) species) within the support framework (MCM-41) was expanded for use of promoters onto the surface of noble metals, directly.

In this regards, a series of Sn(IV) species doping DFNS (designated as SnD) with different Si/Sn ratios were synthesized by the DHS method, and used to fabricate SnD supported $BaMnO_3$ nanoparticles ($BaMnO_3$/SnD) catalysts by in situ reduction of $BaMnO_3$ on the SnD surface. The considering Sn(IV) species within DFNS may be dramatically used as nanocatalyst in the case of the $BaMnO_3$/SnD catalyst to the *N*-formylation of amines through hydrogenation of CO_2. This demonstrated the positive promoting influences of Sn(IV) species.

2 Experimental

2.1 Total Approaches for the Preparation of SnD NPs

2.5 g of TEOS is dissolved in 30 mL cyclohexane and 1.5 mL 1-pentanol solution. After that, $SnCl_4{\cdot}5H_2O$ (with amount of 0.3 g), 1 g stirred solution of cetylpyridinium bromide (CPB) and also 0.6 g urea in water (30 mL) is released. The obtaining mixture is stirred, continually, for 45 min under the temperature of 25 °C and after that placed in a Teflon-sealed hydrothermal reactor and then heated up to the temperature of 120 °C for 300 min. The silica constructed is isolated using centrifugation and then washed by acetone and deionized water and dried (in a drying oven). Under the temperature of 550 °C and for 300 min in air, it was calcined.

2.2 Total Approaches for the Preparation of $BaMnO_3$/SnD NPs

A constant amount of potassium permanganate (0.70 g) liquefied in DI water (15 mL) for acquiring a purple liquid and then carried in the frozen water. An amount of KOH (1.4 g) released in the upper mentioned solution and after that agitated for 20 min in order to complete the reaction with pH stabilized at 12.0.3 g SnD and 2.54 g $Ba(NO_3)_2$, 1.48 g $MnCl_2$ (In a distinct beaker) liquefied in DI water (5 mL). Under ultrasonic radiation, we have mixed the solution to the alkali solution of $KMnO_4$(drop-wise). By ultrasonic

radiation, the composition irradiated for 30 min. Then we released a constant quantity of DI water in upper mentioned solution and after that it was irradiated for 30 min. In order to stop the reaction and decrease the pH to 7, a large amount of deionized water was added to the solution. By using Büchner funnel, the precipitate purified and then washed by ethyl alcohol and deionized water. The compositions dried at the temperature of 75 °C for 2 h. Finally, we calcined the precipitate at the temperature of 400 °C for 4 h.

2.3 General Approach to the Catalytic *N*-Formylation of Amines

At the first step, a glass reactor liner (50 mL) is charged with the amines (15 mmol) and 1,4-dioxane (5 mL) in a glove box. Then, 0.4 mol% of $BaMnO_3$/SnD is added to the compound. The Parr reactor was sealed and deleted from it. The reactor is pressurized by CO_2 under the pressure of 2.5 MPa followed by H_2 (with pressure of 2.5 Mpa) and the temperature is increased to 100 °C. The reactor is cooled using submersion in a bath of ice after 30 min and the remaining gas is vented, slowly. After the reaction completion, for later recycling experiments, the catalyst is separated utilizing a magnet to be more utilized. After drying the resultant crude product onto anhydrous sodium sulphate, the compound is considered to Column Chromatography (CC) via a petroleum ether/EtOAc system that is an eluent (6:1) on silica gel. For recycling procedure, catalyst was obsoleted using filtration and also it's washed with alcohol and dried with the pump. It's added to the main text.

Compound 1 ^{1}H NMR (500 MHz, $CDCl_3$): δ (ppm) 8.04 (s, 1H), 3.01 (s, 3H), 2.92 (s, 3H).

Compound 2 ^{1}H NMR (500 MHz, $CDCl_3$): δ (ppm) 8.01 (s, 1H), 3.32 (q, J = 8.0 Hz, 2H), 3.30 (q, J = 8.0 Hz, 2H), 1.21 (t, J = 8.0 Hz, 3H), 1.15 (t, J = 8.0 Hz, 3H). ^{13}C NMR (125 MHz, $CDCl_3$): δ (ppm) 162.5, 41.9, 36.9, 14.9, 13.1.

Compound 3 ^{1}H NMR (500 MHz, $CDCl_3$): δ (ppm) 8.01 (s, 1H), 3.22–3.10 (m, 4H), 1.57–1.43 (m, 4H), 0.88–0.81 (m, 6H). ^{13}C NMR (125 MHz, $CDCl_3$): δ (ppm) 162.9, 49.6, 44.1, 21.8, 20.5, 11.1, 10.6.

Compound 4 ^{1}H NMR (500 MHz, $CDCl_3$): δ (ppm) 8.47 (s, 1H), 7.51–7.40 (m, 6H), 7.32–7.28 (m, 4H), 4.48 (s, 2H), 4.31 (s, 2H). ^{13}C NMR (125 MHz, $CDCl_3$): δ (ppm) 162.4, 136.3, 135.5, 129.1, 128.5, 128.4, 128.0, 127.4, 127.2, 50.2, 45.0.

Compound 5 ^{1}H NMR (500 MHz, $CDCl_3$): δ (ppm) 8.29 (s, 1H), 3.47 (t, J = 6.43 Hz, 2H), 3.45 (t, J = 6.43 Hz, 2H), 1.98–1.92 (m, 4H) ppm; 13C NMR (100 MHz, CDCl3) δ 160.9, 46.0, 43.1, 24.9, 24.2

Compound 6 ^{1}H NMR (500 MHz, $CDCl_3$): δ (ppm) 7.98 (s, 1H), 3.42 (t, J = 5.54 Hz, 2H), 3.28 (t, J = 5.51 Hz, 2H), 1.72–1.49 (m, 6H). ^{13}C NMR (125 MHz, $CDCl_3$): δ (ppm) 161.0, 46.7, 40.9, 26.3, 24.8, 24.3.

Compound 7 ^{1}H NMR (500 MHz, $CDCl_3$): δ (ppm) 8.02 (s, 1H), 3.69 (dt, J = 14.20, 4.85 Hz, 4H), 3.60–3.56 (m, 2H), 3.39–3.36 (m, 2H). ^{13}C NMR (125 MHz, $CDCl_3$): δ (ppm) 160.6, 67.5, 66.2, 45.9, 40.3.

Compound 8 ^{1}H NMR (500 MHz, $CDCl_3$): δ (ppm) 8.04 (s, 1H), 7.19 (t, J = 7.80 Hz, 2H), 6.89–6.84 (m, 3H), 3.65 (t, J = 5.05 Hz, 2H), 3.42 (t, J = 5.05 Hz, 2H), 3.11 (dt, J = 15.10, 5.05 Hz, 4H). ^{13}C NMR (125 MHz, $CDCl_3$): δ (ppm) 160.9, 151.0, 129.4, 120.7, 116.9, 50.5, 49.1, 45.2, 40.0.

Compound 9 ^{1}H NMR (500 MHz, $CDCl_3$): δ (ppm) 8.90 (s, 1H), 8.48 (dd, J = 146.3, 6.5 Hz, 2H), 7.98 (s, 1H), 7.57 (d, J = 7.8 Hz, 2H), 7.35 (dt, J = 13.8, 8.0 Hz, 4H), 7.23–7.11 (m, 2H). ^{13}C NMR (125 MHz, $CDCl_3$): δ (ppm) 163.8, 159.2, 137.0, 129.6, 128.7, 125.6, 125.0, 119.8, 118.6.

Compound 10 ^{1}H NMR (500 MHz, $CDCl_3$): δ (ppm) 8.49 (d, J = 11.8 Hz, 1H), 8.33 (m, 2H), 7.51 (br, 1H), 7.47 (d, J = 8.9 Hz, 2H), 7.07 (d, J = 8.7 Hz, 2H), 6.89–6.82 (m, 4H), 3.79 (s, 6H). ^{13}C NMR (125 MHz, $CDCl_3$): δ (ppm) 161.1, 159.2, 157.5, 157.0, 130.2, 129.9, 122.0, 121.8, 114.9, 114.5, 55.8, 55.7.

Compound 11 ^{1}H NMR (500 MHz, $CDCl_3$): δ (ppm) 8.41 (s, 1H), 7.30 (t, J = 7.8 Hz, 2H), 7.18 (t, J = 7.2 Hz, 1H), 7.07 (d, J = 7.8 Hz, 2H), 3.25 (s, 3H). ^{13}C NMR (125 MHz, $CDCl_3$): δ (ppm) 162.6, 142.4, 129.8, 126.5, 122.3, 32.4.

3 Results and Discussion

In the Scheme 1, it can be seen that, for production of $BaMnO_3$/SnD nanocatalysts, many stages have to be conducted. The fibers of DFNS involve Si–OH bond groups on the sites. Hence, it is expected that the DFNS is functionalized using Sn(IV) for forming SnD. The quantity of extracted Ananas comosus was varied to discover its effect on $BaMnO_3$ dimension, catalytic yield, and shape.

The fibers of DFNS involve many bonds of Si–OH on the sites. Therefore, it is expected that the fibers of DFNS is easily functionalized utilizing Sn(IV) to construct SnD.

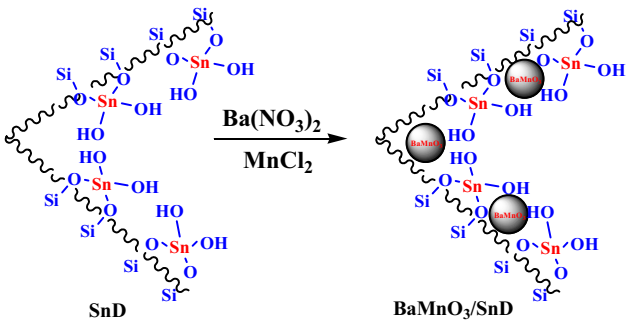

Scheme 1 Schematic illustration of the $BaMnO_3$/SnD NPs preparation

Moreover, the Sn groups on the SnD maybe utilized as association centers in the case of the $BaMnO_3$ nanoparticles formation on the DFNS fibers site. As can be seen in Fig. 1, TEM and SEM schemes about the SnD, $BaMnO_3$/SnD, and DFNS catalysts. Figure 1a and d shows that the DFNS NPs had an association size of particle rate about 250 nm. Therefore, for making SnD core–shell particles (as seen in Fig. 1b and e) hyperbranched Sn(IV) was coated on the DFNS. Moreover, after anchoring the $BaMnO_3$, the metal nanoparticles were obviously differentiable using the diversity in their contrast. The as-gathered nanoparticles of metal were spherical without significant aggregation. As can be seen in Fig. 1c and f, the nanoparticles morphology was near-wall $BaMnO_3$. In addition, the diameter of NPs was about 20–30 nm.

Figure 2 shows the XRD schema in the case of $BaMnO_3$/SnM catalysts at low and high angles. For examining the as-achieved nanostructured $BaMnO_3$, we have used XRD analysis that may be considerably beneficial approach in term of detection of mean crystallite size as well as crystalline structure. The broad peak in the range of 20–30° shows amorphous silica. As can be seen in Fig. 2, the diffraction peaks are clear and whole are properly matched with pure fluorite $BaMnO_3$. In addition, there exist no impurities. These patterns were in perfect accord with the Hexagonal Phase $BaMnO_3$ (JCPDS card No. 26-0168).

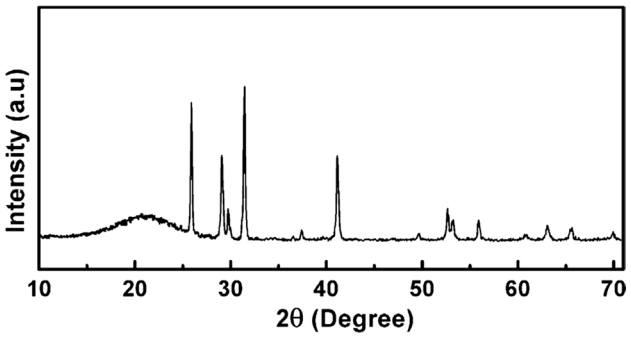

Fig. 2 XRD analysis of $BaMnO_3$/SnD NPs

The spectra of XPS for Si, Sn, and O in catalysts of $BaMnO_3$/SnD were demonstrated in Fig. 3. Noted that $BaMnO_3/SnO_2$ as well as $BaMnO_3$/SnD catalysts were utilized as references. As seen in Fig. 3a, there are two typical doublets with the binding energies of ca. 484−486 eV and ca. 493−495 eV that may be considered to the $3d_{3/2}$ and $3d_{5/2}$ peaks in term of Sn^{4+}, respectively [20].The Sn $3d_{5/2}$ peaks of $BaMnO_3$/SnD varies to high binding energy (486–487 eV) [22] in comparison with the Sn $3d_{5/2}$ peak of $BaMnO_3/SnO_2$, 486 eV, indicating the Sn–O–Si bonds formation in SnM support. Figure 3b shows two deconvoluted peaks related to O 1 s peak for $BaMnO_3$/DFNS at 532.2 eV,

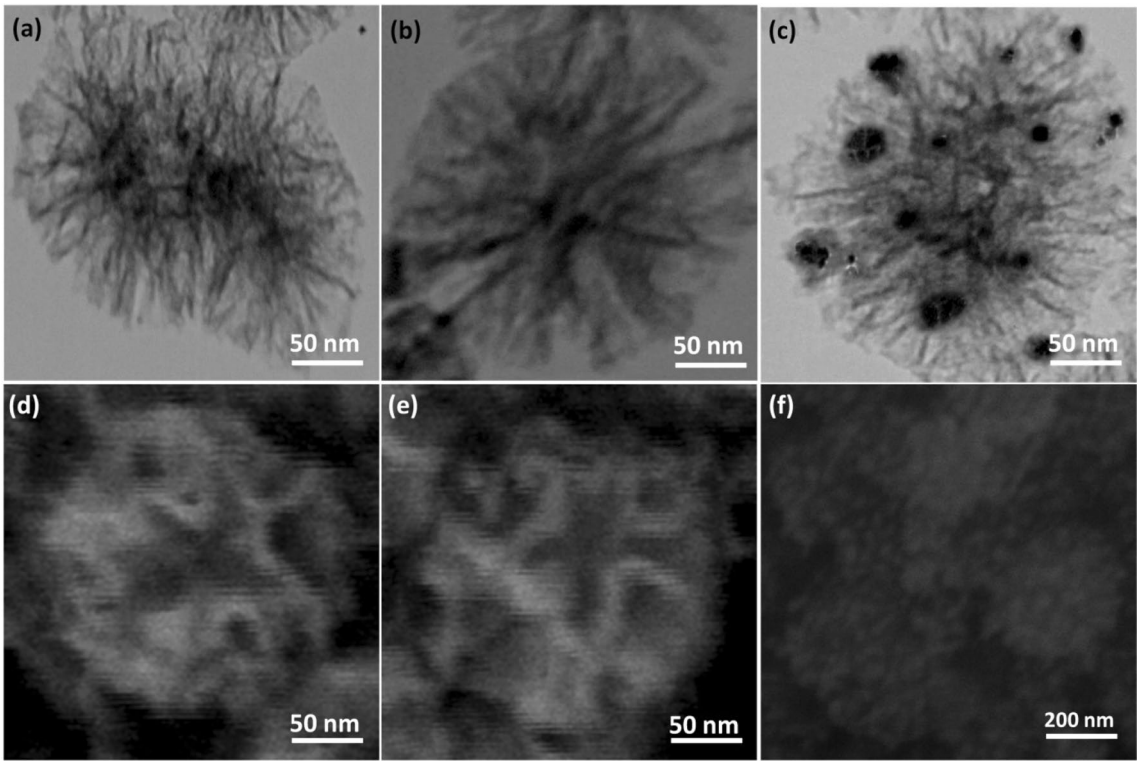

Fig. 1 TEM images of DFNS (**a**); SnD (**b**); $BaMnO_3$/SnD (**c**); SEM images of DFNS (**d**); SnD (**e**); $BaMnO_3$/SnD (**f**)

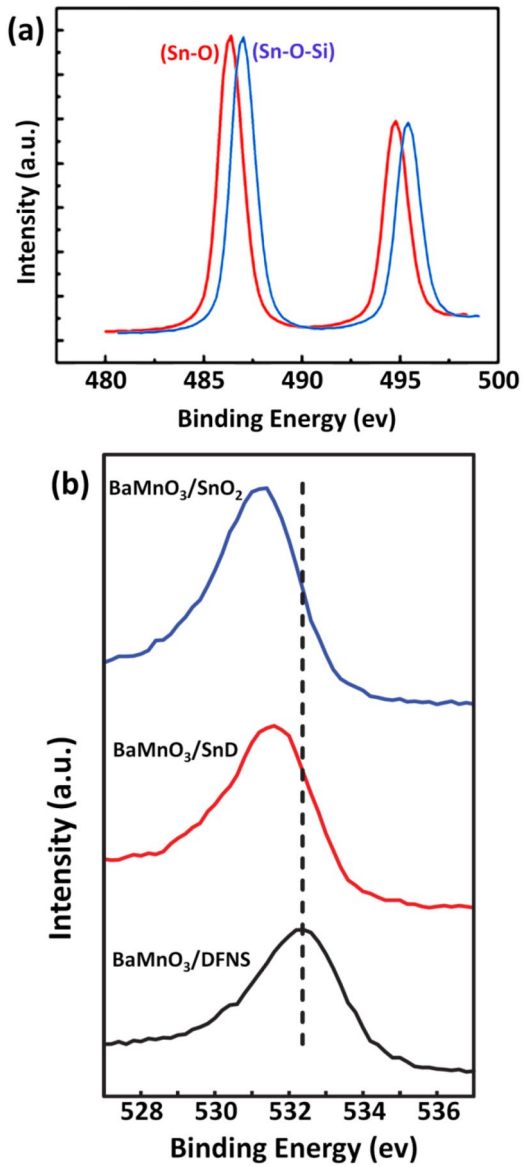

Fig. 3 XPS spectra of $BaMnO_3$/DFNS, $BaMnO_3$/SnD, and $BaMnO_3$/SnO_2, **a** Sn, and **b** O spectra

assigning to bonds of O−Si [21, 23] and a peak in $BaMnO_3$/SnD that was assigned to O−Si (531.1 eV) bond [23, 24]. At 530.9 eV, larger zone of the O−Sn peak was seen that is related to $BaMnO_3$/SnO_2, showing more O−Sn bonds existence on $BaMnO_3$/SnO_2 surfaces can be because of the formation of SnO_2 crystallites.

BET specific surface area for $BaMnO_3$/SnD and SnD are specified through analysis of nitrogen physisorption and determined that specific surface area was equal to 548, and 211 $m^2\ g^{-1}$, respectively. $BaMnO_3$/SnD had a reduction compared to SnD in surface area. It can be because of the supporting of $BaMnO_3$ in the SnD. In addition, the surface area reduction is more clear in $BaMnO_3$/SnD nanoparticles

Table 1 Structural parameters of DFNS, and $BaMnO_3$/SnD NPs

Catalysts	S_{BET} ($m^2\ g^{-1}$)	V_a ($cm^3\ g^{-1}$)	D_{BJH} (nm)
SnD	548	3.2	11
$BaMnO_3$/SnD	211	1.1	2

due to poor bicontinuous concentric $BaMnO_3$ morphology in the case of the nanocatalyst. In SnD, the attendance of mesopores was proved by the presence of IV isotherm as well as H1-type hysteresis loop. In order calculate the pore size distribution, the desorption branch of nitrogen isotherm was utilized with BJH approach. As seen in Table 1, we determined that, at 11 nm, relating pore size distribution showed a narrow pore size distribution peaked (refer to Table 1). The great mesopore size of SnD with great capacity can load $BaMnO_3$ that have relative large molecular size.

The reaction conditions are optimized by applications of CO_2, pyrimidine, and H_2 for the *N*-formylation of pyrrolidine that is catalyzed by nanoparticles of $BaMnO_3$/SnD in the suggested model approach. The model reaction presented analyzes of the influences of distinct factors as seen in Table 2. Different solvents are used to investigate their effects on the $BaMnO_3$/SnD NPs synthesis (refer to Table 2, Entries 1–18). Our outcomes showed no formation of the attended product by polar protic solvents like water, methanol, and isopropanol, as well as ethanol. The cross-coupling product demonstrated a relatively average-to-good yield by DMSO, EtOAc, and DMF that considered as the polar aprotic solvents. As seen in Table 2, Entry 10, 1,4-dioxane is detected as a more efficient substance compared to the other solvents. The catalyst amount for the reaction is known as an important parameter that have to be consider in the current reaction. No product is achieved in the lack of the catalyst. Moderate products are obtained by the adding 0.2–1 mol% of catalyst within the sample reaction. In the attendance of a constant amount of catalyst (0.4 mol%), when the model reaction is done, the best result is achieved. It should be to note that the model reaction is not enhanced with enhancing the catalyst amount.

N-formylation yield is increased quickly with enhancing the time of reaction up to 20 min, after that this approach is observed to decline. The extended reactions showed a further again to 30 min that is the highest transformation is established. The products of pyrrolidine-1-carbaldehyde are decreased again beyond this time. It is observed that the viscosity of reaction system is increased with the formation of pyrrolidine-1-carbaldehyde that caused in the interplay obstruction among the reactants and catalyst at a longer time more than (30 min). Figure 6 shows the products of the *N*-formylation of pyrrolidine against the time of reaction.

Figure 7 shows the pyrrolidine-1-carbaldehyde product that illustrated among 35 °C and 100 °C. It is found that

Table 2 The *N*-formylation of pyrrolidine by using $BaMnO_3$/SnD NPs in different solvents

Entry	Solvent	Catalyst (mol%)	T (°C)	Yield (%)[a]
1	H_2O	1.0	105	–
2	MeOH	1.0	65	–
3	EtOH	1.0	80	–
4	*i*-PrOH	1.0	80	–
5	DMA	1.0	120	88
6	DMF	1.0	120	71
7	THF	1.0	65	40
8	CH_2Cl_2	1.0	40	65
9	$CHCl_3$	1.0	60	69
10	CCl_4	1.0	75	–
11	CH_3CN	1.0	80	22
12	EtOAc	1.0	75	51
13	DMSO	1.0	120	65
14	Anisole	1.0	120	18
15	Toluene	1.0	110	38
16	*n*-Hexane	1.0	70	–
17	Cyclohexane	1.0	80	–
18	solvent-free	1.0	100	–
19	1,4-Dioxane	1.0	100	97
20	1,4-Dioxane	0.8	100	97
21	1,4-Dioxane	0.4	100	97
22	1,4-Dioxane	0.2	100	84

Reaction conditions: pyrrolidine (15 mmol), solvents (15 mL), H_2 2.0 Mpa, and CO_2 2.0 MPa

[a]Isolated yields

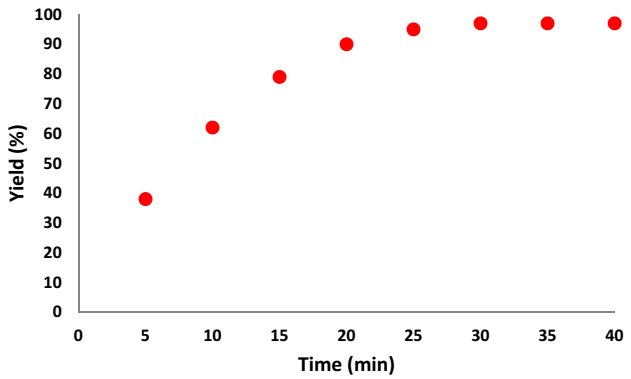

Fig. 6 The effect of time on the *N*-formylation of pyrrolidine

the catalyst activity is dramatically affected with varying the temperature of reaction. The high temperature is proper for the pyrrolidine-1-carbaldehyde production implied the favorable thermodynamic coupling reactions. The products of pyrrolidine-1-carbaldehyde significantly enhanced from 18 to 96% by increasing the temperature of

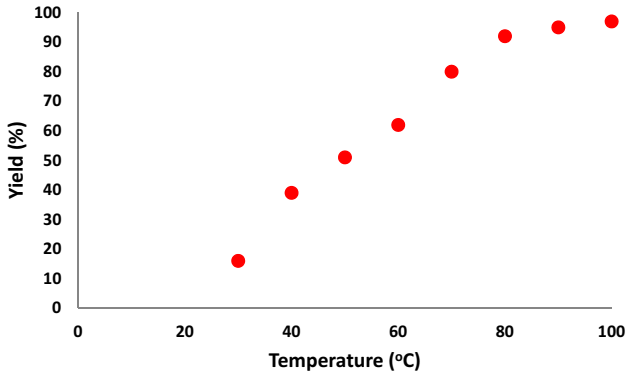

Fig. 7 The effect of temperature on the *N*-formylation yield of product

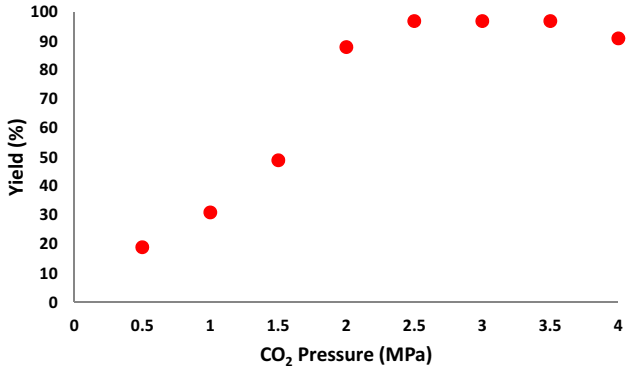

Fig. 8 The effect of CO_2 pressure on the synthesis of product

reaction from 35 to 100 °C so showing the utility of high temperatures for the favorable coupling reaction.

In addition, for optimizing the *N*-formylation product of pyrrolidine and analyze the catalytic efficiency of $BaMnO_3$/SnD NPs, the pressure of carbon dioxide is studied. The optimal pressure of it to provide the maximum product of $BaMnO_3$/SnD NPs should be determined because the kinetics of the mass transfer reactions had to be influenced by the reaction as well as the diffusion among pyrrolidine, H_2, and CO_2. The pressure influences in the range of 0.5–4.0 Mpa are investigated. The $BaMnO_3$/SnD NPs yield sharply enhanced while the pressure of CO_2 increased from 1.5 to 2.0 Mpa. After that $BaMnO_3$/SnD NPs yield was constant in the pressure range of 2.5–3.5 MPa (refer to Fig. 8). Nevertheless, a decreased product is achieved when the pressure was around 4.0 MPa. In the reaction system, it could be illustrated using the pyrrolidine-1-carbaldehyde yield enhance induced with higher pressure of CO_2 and its further concentration increase in the low-pressure. Yet, the product should be reduced with its high pressure that could decrease concentration of pyrrolidine in the catalyst vicinity, whereas pyrrolidine itself can additionally use as an its

declined concentration and reactant could be unfavorable for the reaction. For the maximum yields of pyrrolidine-1-carbaldehyde, these contrary facts showed the need for pressure of 2.5 MPa as an optimum pressure (refer to Fig. 8). Furthermore, the fundamental role of the pressure of H_2 in the *N*-formylation of pyrrolidine in the attendance of the nanoparticles of $BaMnO_3$/SnD as the catalyst. The *N*-formylation of pyrrolidine is studied at the H_2 pressure in the range of 0.5–4.0 bar at isobaric conditions to investigate the pressure effects. In a pressure range (from 2.5 to 4.0 bar), there are no significant influences of pressure on the products of pyrrolidine-1-carbaldehyde. Our obtained outcomes showed that the pyrrolidine-1-carbaldehyde synthesis in the attendance of $BaMnO_3$/SnD NPs are already done causing in proper yields (97%) with a constantly enhancing pressure (2.5 bar and more) (refer to Fig. 9).

For optimizing the conditions of reaction, this methodology is analyzed utilizing distinct amines in the attendance of $BaMnO_3$/SnD NPs at the same conditions so as to define the efficiency of this method by taking into consideration of the library construction, particularly. The various amines do not indicate significantly clear influences on the products for the reaction conditions as can be observed in Table 3. The 3-component reaction showed a smooth measuring approach (refer to Table 3). When utilized from aromatic amines the yields are obtained at the similar conditions (refer to Table 3, entries 9–11).

The comparisons of the catalytic activity of $BaMnO_3$/SnD with other recent catalysts used for *N*-formylation amines with utilization of CO_2 as a C1 source (Table 4). The results showed that our catalyst system had the highest yield of formamide for the same reaction time, although a catalytic amount of base was required, which confirmed that our catalyst was more active.

The reusability state of a catalyst has been introduced as a considerable property in the green chemistry. Therefore, reusability state of the nanoparticles of the $BaMnO_3$/SnD was studied under an optimized state for *N*-formylation

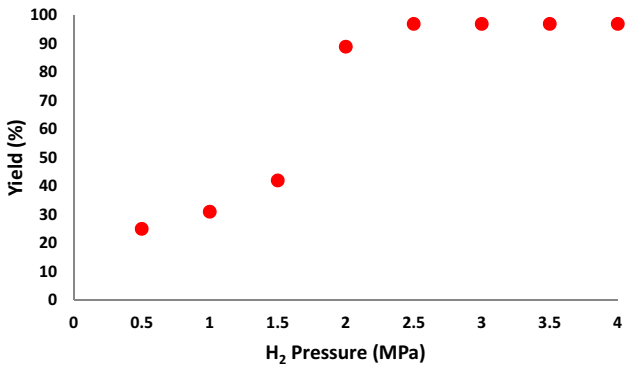

Fig. 9 The effect of H_2 pressure on the synthesis of product

Table 3 Catalysis of *N*-formylation by $BaMnO_3$/SnD NPs via reductive CO_2 hydrogenation

Compound	Substrate	Product	Yield (%)[a]
1		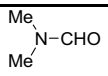	92
2		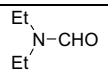	88
3		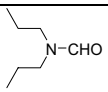	84
4		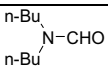	89
5		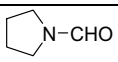	97
6		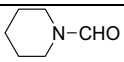	95
7		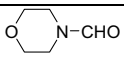	90
8	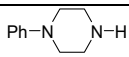	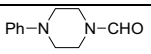	98
9	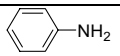	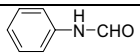	83
10	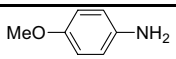	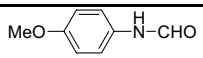	74
11	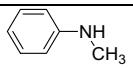	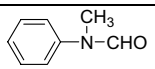	86

Reaction conditions: amines (15 mmol), $BaMnO_3$/SnD NPs (0.4 mol %), 1,4-dioxane (15 mL), H_2 2.5 MPa, and CO_2 2.5 MPa for 40 min at 100 °C

[a]Isolate

through reductive carbon dioxide hydrogenation. The $BaMnO_3$/SnD NPs were separated, directly, of the liquid reaction area, this compound readily separates from the solution after only a few seconds of performing the reaction. It can may be reused, quickly, after solvent cleaning. As can be seen in Fig. 10, the catalyst was reused for 10th continuous runs. The obtained product was 92% at the ten run, which indicates just a 5% drop in performance

Table 4 Comparison of the catalytic efficiency of $BaMnO_3$/SnD NPs with various catalysts

Entry	Catalyst	Experimental conditions	Yield (%)
1	NHC-Ir COD complex	100 °C, 20 h, 30 bar CO_2/30 bar H_2	94 [42]
2	Ru complex	90 °C, 30 h, 40 bar CO_2/40 bar H_2	70 [43]
3	Cu(II) complex	90 °C, 1.5 h, 15 bar CO_2/20 bar H_2	94 [44]
4	Pd/NC-800-6.9%	130 °C, 24 h, 30 bar CO_2/40 bar H_2	84 [45]
5	$Cu_2(OH)_2CO_3$	130 °C, 24 h, 30 bar CO_2/40 bar H_2	94 [46]
6	Carpy-CMP@Ru	130 °C, 24 h, 40 bar CO_2/40 bar H_2	90 [47]
7	Co-pincer complex	150 °C, 36 h, 30 bar CO_2/30 bar H_2	93 [48]
8	$Co(ClO_4)_2$. $6H_2O$, PPh_3	140 °C, 24 h, 30 bar CO_2/30 bar H_2	94 [49]
9	$BaMnO_3$/SnD	100 °C, 30 min, 2.5 bar CO_2/2.5 bar H_2	97 [this work]

Reaction conditions: pyrrolidine in different temperature, time, and pressure of CO_2 and H_2

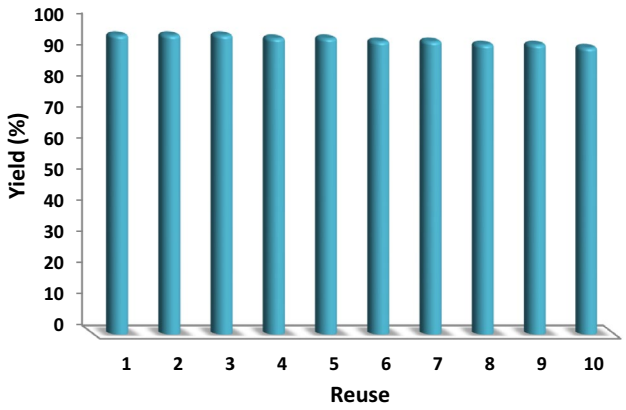

Fig. 10 The reusability of catalysts for synthesis of 3-aryl-2-Oxazolidinone

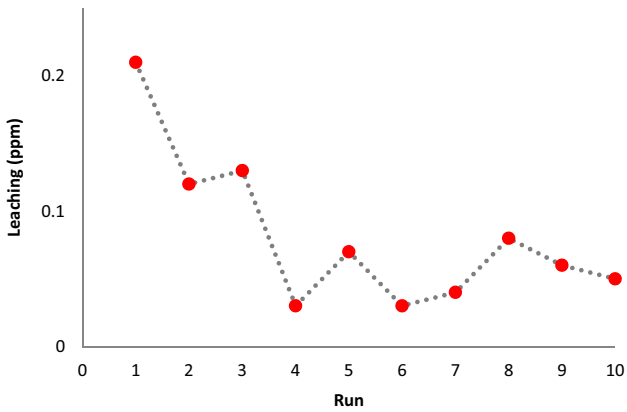

Fig. 11 Recyclability of the catalyst for *N*-formylation via reductive CO_2 hydrogenation

was observed compared to the related fresh catalyst (97%). Furthermore, after each run, for *N*-formylation the amount of iron leached into the solution was analyzed by ICP. Reusing the catalyst in 10 consecutive cycles (Fig. 11) did not result in any loss in catalytic activity with minimal (< 0.03 ppm) leaching of iron (assessed by ICP-OES).

Furthermore, to illustrate the catalyst heterogeneous nature, a complete investigation was done. In the first step, we have performed the hot filtration experiment for to the *N*-formylation and indicated that the catalyst was deleted after by 62% at 20-min removal in situ. The reactants were allowed to with stand more reaction. The results illustrated that the free catalyst remnant was weakly active, after taking the heterogeneous catalyst. The conversion around 63% was achieved after 50 min of the product. During the reaction, we have proved that the catalyst acted, heterogeneously, and unwilling only slight leaching performed in the reaction. In the second step, in order to ensure the heterogeneous pattern of the catalyst, the mercury poisoning investigation was additionally done. Mercury (0) was imbibed as using synthesis or a metal. Furthermore, Mercury (0) was considerably deactivated the metal catalyst (active surface) and also tranquilized the catalyst activity. Our experiments proved the heterogeneous catalyst and is done with the upper-mentioned model of reaction at optimized conditions. Around 300 molar mercury was added to the compound of reaction after 20 min of the reaction. The reaction area was stirred for more than 50 min. In the mentioned reaction, no more conversion was observed after 50 min from poisoning the catalyst. Figure 12 shows a kinetics figure of the reaction at the presence of Hg(0). The negative results achieved from the total heterogeneity experiments (Hg(0) poisoning and also hot filtration) suggested that the solid catalyst was actually heterogeneous and no obtainable iron leaching acted upon *N*-formylation.

4 Conclusion

In this paper, a series of catalysts of $BaMnO_3$/SnD were synthesized using in situ $BaMnO_3$ on the synthesized SnD surface. The catalysts of $BaMnO_3$/SnD had appropriate mesoporous structure as well as the Sn(IV) species

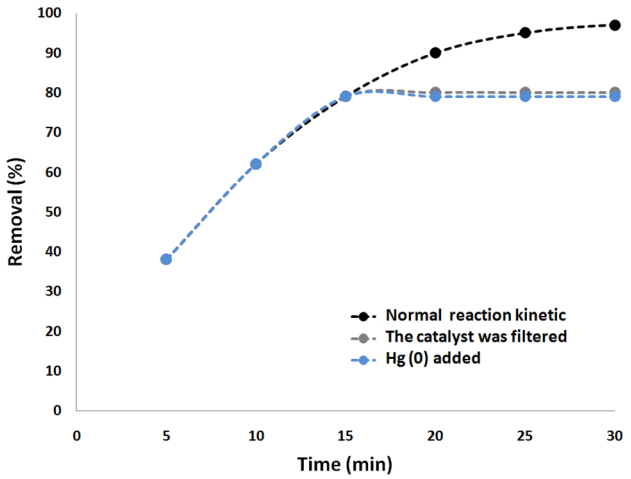

Fig. 12 Reaction kinetics, Hg (0) poisoning, and hot filtration studies for *N*-formylation

were properly incorporated within the SnD frame work. Enhancing the amount of Sn doping was useful to form little $BaMnO_3$ particles and enhancing the catalysts surface basicity. When the catalytic *N*-formylation via reductive CO_2 hydrogenation onto $BaMnO_3$/SnD catalysts performed, the $BaMnO_3$ NPs run as the active site and the species of Sn(IV) as the promoter.

Acknowledgements This work was financially supported by the National Natural Science Foundation of China (Grant No.: 51701173) and the Key Scientific and Technological Research Project of Henan Province (Grant No.: 202102310298).

References

1. Dibenedetto A, Angelini A, Stufano P (2014) J Chem Technol Biotechnol 89:334–353
2. Low JX, Cheng B, Yu JG (2017) Appl Surf Sci 392:658–686
3. Boot-Handford ME, Abanades JC, Anthony EJ, Blunt MJ, Brandani S, Mac Dowell N, Fernandez JR, Ferrari MC, Gross R, Hallett JP, Haszeldine RS, Heptonstall P, Lyngfelt A, Makuch Z, Mangano E, Porter RTJ, Pourkashanian M, Rochelle GT, Shah N, Yao JG, Fennell PS (2014) Energy Environ Sci 7:130–189
4. Devens G, Moore TA, Moore AL (2009) Acc Chem Res 42:1890–1898
5. Morris AJ, Meyer GJ, Fujita E (2009) Acc Chem Res 42:1983–1994
6. Morimoto T, Nishiura C, Tanaka M, Rohacova J, Nakagawa Y, Funada Y, Koike K, Yamamoto Y, Shishido S, Kojima T, Saeki T, Ozeki T, Ishitani O (2013) J Am Chem Soc 135:13266–13269
7. Sadeghzadeh SM, Zhiani R, Emrani S (2018) Appl Organomet Chem 32:e3941
8. Benson EE, Kubiak CP, Sathrum AJ, Smieja JM (2009) Chem Soc Rev 38:89–99
9. Sadeghzadeh SM (2015) RSC Adv 5:68947–68952
10. Thoi VS, Chang CJ (2011) Chem Commun 47:6578–6580
11. Sadeghzadeh SM (2016) Catal Sci Technol 6:1435–1441
12. Qu Y, Duan X (2013) Chem Soc Rev 42:2568–2580
13. Chowdhury AH, Chowdhury IH, Biswas S, Islam SKM (2020) Mol Catal 493:111050
14. Mu J, Liu J, Ran Z, Arif M, Gao M, Wang C, Ji S (2020) Ind Eng Chem Res 59:6543–6555
15. Wang G, Jiang M, Ji G, Sun Z, Li C, Yan L, Ding Y (2020) ACS Sustain Chem Eng 8:5576–5583
16. Dai X, Shi F (2020) Curr Opin Green Sustain Chem 22:1–6
17. Nale DB, Bhanage BM (2016) Synlett 27:1413–1417
18. Lv H, Xing Q, Yue C, Lei Z, Li F (2016) Chem Commun 52:6545–6548
19. González-Sebastián L, Flores-Almo M, García J (2015) J Organomet 34:763–769
20. Nguyen TVQ, Yoo WJ, Kobayashi S (2015) Angew Chem Int Ed 54:9209–9212
21. Jacquet O, Frogneux X, Gomes CDN, Contat T (2013) Chem Sci 4:2127–2131
22. Jacquet O, Gomes CDN, Ephritikhine M, Contat T (2013) ChemCatChem 5:117–120
23. Cui X, Zhang Y, Deng Y, Shi F (2014) Chem Commun 50:189–191
24. Ju P, Chen J, Chen A, Chen L, Yu Y (2017) ACS Sustain Chem Eng 5:2516–2528
25. Mitsudome T, Urayama T, Fujita S, Maeno Z, Mizugaki T, Jitsukawa K, Kaneda K (2017) ChemCatChem 9:3632–3636
26. Kumar S, Jain SL (2014) RSC Adv 4:64277–64279
27. Song QW, Zhou ZH, He LN (2017) Green Chem 19:3707–3728
28. Gholamrezaei S, Salavati-Niasari M (2018) Ultrason Sonochem A 40:651–663
29. Melo Jorge ME, Nunes MR, Silva Maria R, Sousa D (2005) Chem Mater 17:2069–2075
30. Isasi PH, Lopes ME, Nunes MR, Melo Jorge ME (2009) J Phys Chem Solids 70:405–411
31. Sakintuna B, Lamari-Darkrim F, Hirscher M (2007) Int J Hydrog Energy 32:1121–1140
32. Fukabori A, Awaka J, Takahashi Y, Kijima N, Hayakawa H (2008) J. Akimoto. Chem Lett 37:978–979
33. Haghiri-Gosnet AM, Renard JP (2003) J Phys D 36:127–130
34. Battle PD, Gibb TC, Jones CW (1988) J Solid State Chem 74:60–67
35. Zhu D, Zhu H, Zhang Y (2002) Appl Phys Lett 80:1634–1636
36. Sakai H (2011) Phys Rev Lett 107:137601
37. Ouyang J (2019) Nano Mater Sci 1:77–90
38. Masjedi-Arani M, Salavati-niasari M (2018) Ultrason Sonochem 43:136–145
39. Masjedi-Arani M, Salavati-niasari M (2016) Ultrason Sonochem 29:226–235
40. Corma A, Navarro Ma T, Renz M (2003) J Catal 219:242–246
41. Chaudhari K, Das TK, Rajmohanan PR, Lazar K, Sivasanker S, Chandwadkar AJ (1999) J Catal 183:281–291
42. Zhang Y, Wang J, Zhu H, Tu T (2018) Chem Asian J 13:3018–3021
43. Zhang FH, Liu C, Li W, Tian GL, Xie JH, Zhou QL (2018) Chin J Chem 36:1000–1002
44. Zhiani R, Saadati SM, Zahedifar M, Sadeghzadeh SM (2018) Catal Lett 148:2487–2500
45. Luo X, Zhang H, Ke Z, Wu C, Guo S, Wu Y, Yu B, Liu Z (2018) Sci China Chem 61:725–731
46. Li XD, Xia SM, Chen KH, Liu XF, Li HR, He LN (2018) Green Chem 20:4853–4858
47. Yang Z, Wang H, Ji G, Yu X, Chen Y, Liu X, Wu C, Liu Z (2017) New J Chem 41:2869–2872
48. Daw P, Chakraborty S, Leitus G, Diskin-Posner Y, Ben-David Y, Milstein D (2017) ACS Catal 7:2500–2504
49. Liu Z, Yang Z, Ke Z, Yu X, Zhang H, Yu B, Zhao Y, Liu Z (2018) New J Chem 42:13933–13937